Journal Name

ARTICLE TYPE

Cite this: DOI: 00.0000/xxxxxxxxxx

Pressure effects on the anomalous thermal transport and anharmonic lattice dynamics of CsX (X = Cl, Br, I)†

Shasha Li,[a] Zezhu Zeng,[b] Yong Pu,*[a,c] and Yue Chen*[b]

Received Date
Accepted Date

DOI: 00.0000/xxxxxxxxxx

The lattice thermal conductivity of CsX (X = Cl, Br, I) and its pressure dependence are investigated using first-principles third-order anharmonic force constants. Contrary to the expectation that compounds with heavier atoms usually exhibit lower lattice thermal conductivity (k_L), the k_L of CsI is higher than those of CsCl and CsBr. This anomalous behavior is examined by analyzing the group velocity, phonon lifetime, three-phonon scattering phase space and Grüneisen parameters. The higher k_L of CsI can be attributed to its longer phonon lifetimes due to weaker absorption processes in the range of 1 $\sim$ 2.1 THz. It is found that the lattice thermal conductivity of CsI is more sensitive to hydrostatic pressure, and the k_L of CsI becomes lower than those of CsCl and CsBr at -2 GPa due to the shorter phonon lifetimes and the smaller group velocities. Moreover, the changes of bulk modulus and Bader charge of CsX are also discussed to provide further insight into the anomalous thermal behavior.

1 INTRODUCTION

Materials with ultralow lattice thermal conductivities (k_L) have attracted great attention due to their potential applications, such as thermoelectrics [1–6]. Generally, ultralow k_L is often found in materials with complex crystal structures [1–3] or intrinsic lattice instability [4,5]. Despite the very simple cubic crystal structure (space group: $Pm\bar{3}m$), cesium halides CsX (X = Cl, Br, I) exhibit very low k_L, and their room-temperature k_L are below 1 W/mK [7], which is even lower than that of the widely studied thermoelectric PbTe (2.2 W/mK) [1]. The experimental room-temperature k_L of CsI is higher than those of CsCl and CsBr [7], which is contrast to the general expectation that crystals with heavier atoms usually exhibit lower k_L [8]. However, the origin of this anomalous thermal behavior of CsX is not yet fully understood.

An in-depth study of the anharmonic lattice dynamics is crucial to uncover the intrinsic lattice thermal transport mechanism. Strong transverse optical (TO) and longitudinal acoustic (LA) phonon coupling was found to play an important role in the low k_L of PbTe [4]. The low k_L of SnSe was attributed to the giant phonon couplings originated from the ferroelectric-like lattice instability [5]. The low k_L of Te was reported to be related to the short phonon lifetimes of low-frequency acoustic modes [6]. To better understand the origin of the low k_L of CsX, the lattice dynamics of CsCl and CsI were studied recently [9,10]. Through high-resolution X-ray diffraction, Mattia et al. found that the lattice anharmonicity of CsCl at room-temperature is weaker than that at 20 K [9]. Based on first-principles calculations, the k_L of CsCl was studied based on the relaxation time approximation (RTA) and the iterative solution of Boltzmann transport equation (BTE) [11]. By performing inelastic neutron scattering experiments and first-principles calculations, Wei et al. reported that the low k_L of CsI originates from the small phonon group velocities and the large phonon scattering rates [10]. However, a systematic comparative study of the anharmonic lattice dynamics and the thermal transport behavior of CsX is still missing.

Recently, the unexpected thermal transport behavior that heavier compounds exhibit higher k_L has been studied in several systems. Although Te is heavier than Se, $CuInTe_2$ and $AgInTe_2$ exhibit higher k_L than those of $CuInSe_2$ and $AgInSe_2$, respectively, which was attributed to the weaker phonon anharmonicity in tellurides [12]. It was reported that the k_L of $CsSnCl_3$ is lower than that of $CsSnBr_3$, which originates from the short phonon lifetimes in $CsSnCl_3$ [13]. The k_L of CaO was also found to be lower than that of CaS, whereas the k_L of CaO exceeds that of CaS under a compressive strain over 2% [14]. In this work, the anharmonic lattice dynamics of CsX are investigated to elucidate the pressure dependence of k_L of CsX, as well as the unexpected higher k_L of CsI. To have a more comprehensive understanding of the thermal transport behavior of CsX, the phonon group velocities, phonon lifetimes, three-phonon scattering phase space and Grüneisen parameters of CsX are discussed in detail.

[a] School of Science, Nanjing University of Posts and Telecommunications, Nanjing, 210023, China
[b] Department of Mechanical Engineering, The University of Hong Kong, Pokfulam Road, Hong Kong SAR, China
[c] New Energy Technology Engineering Laboratory of Jiangsu Province, Nanjing University of Posts and Telecommunications, Nanjing, 210023, China
* puyong@njupt.edu.cn, yuechen@hku.hk

2 COMPUTATIONAL DETAILS

The k_L of CsX was calculated by solving the BTE within the RTA implemented in ALAMODE with a q-point mesh of $40 \times 40 \times 40$ (the convergence test is given Fig. s1) [15]:

$$\kappa_L^{\mu\nu} = \frac{1}{N\Omega} \sum_{q,j} C_{q,j} v_{q,j}^{u} v_{q,j}^{v} \tau_{q,j} \tag{1}$$

where N and Ω are the number and volume of unit cell, respectively; $C_{q,j}$ and $v_{q,j}$ are the heat capacity and group velocity of mode j at q point, respectively. $\tau_{q,j}$ is the phonon lifetime, corresponding to the reciprocal of phonon linewidth $2\Gamma_{q,j}(\omega_{q,j})$,

$$\tau_{q,j} = \frac{1}{2\Gamma_{q,j}(\omega_{q,j})} \tag{2}$$

$\omega_{q,j}$ is the harmonic phonon frequency obtained via the second-order force constants; $\Gamma_{q,j}(\omega)$ is the imaginary part of phonon self-energy ($\Sigma_{q,j}(\omega) = \Delta_{q,j}(\omega) - i\Gamma_{q,j}(\omega)$), which can be calculated from the third-order anharmonic force constants based on the perturbation theory. $\Delta_{q,j}(\omega)$ describes the frequency shift at elevated temperature, and it can be obtained from $\Gamma_{q,j}(\omega)$ using the Kramers-Kroning relation [6,16]. With the phonon self-energy $\Sigma_{q,j}(\omega)$, the phonon spectrum $\chi_{q,j}(\Omega)$ at elevated temperatures can be calculated using [15]:

$$\chi_{q,j}(\Omega) \propto \frac{4\omega_{q,j}^2 \Gamma_{q,j}(\Omega)}{[\Omega^2 - \omega_{q,j}^2 - 2\omega_{q,j}\Delta_{q,j}(\Omega)]^2 + 4\omega_{q,j}^2 \Gamma_{q,j}(\Omega)^2}. \tag{3}$$

The second-order force constants were calculated using the finite displacement method. The third-order force constants were extracted based on the compressive sensing approach using the least absolute shrinkage and selection operator (LASSO) technique [15,17], which was often used for strongly anharmonic materials [13,18,19]. The third-order force constants were extracted from the following LASSO equation:

$$\arg\min_{\Phi} ||A\Phi - F||_2^2 + \lambda ||\Phi||_1 \tag{4}$$

where A and F are the displacement matrix and force vector, respectively. The A - F datasets were obtained by the following procedures: first, ab initio molecular dynamics (AIMD) simulations in the canonical ensemble (NVT) were performed using $4 \times 4 \times 4$ supercells of CsX for 4 ps with a time step of 2 fs at 300 K; then for 40 atomic configurations equally spaced in time, all the atoms were displaced by 0.1 Å in random directions to include anharmonic terms up to the sixth order when fitting Φ; finally, the atomic forces of these configurations were calculated based on density functional theory (DFT), and the A - F datasets were constructed. The LASSO equation was solved using the split Bregman algorithm [20,21], and the optimal value of λ was selected from the four-fold cross-validation score [19].

All DFT calculations were performed using Vienna ab initio simulation package (VASP) [22] and the energy cutoff was set to 400 eV. The electron-ion interactions were treated with the projector augmented wave (PAW) method [23] and the exchange-correlation interactions were treated with the local density approximation (LDA) functional [24]. The total energy tolerance was set to 10^{-8} eV. A Monkhorst-Pack grid [25] of $3 \times 3 \times 3$ was used for the $4 \times 4 \times 4$ supercells of CsX. Born effective charge and dielectric tensor were calculated based on density functional perturbation theory (DFPT) to consider the non-analytic part of the dynamical matrix.

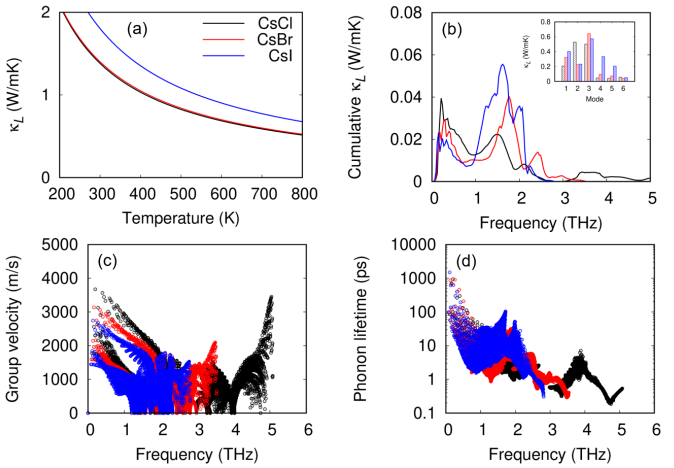

Fig. 1 (a) Temperature-dependent lattice thermal conductivities of CsCl, CsBr and CsI. (b) Cumulative lattice thermal conductivity and mode-dependent lattice thermal conductivity (inset) at 300 K. Phonon modes are ranked from low to high frequency. (c) Phonon group velocities of CsCl, CsBr and CsI. (d) Phonon lifetimes of CsCl, CsBr and CsI at 300 K.

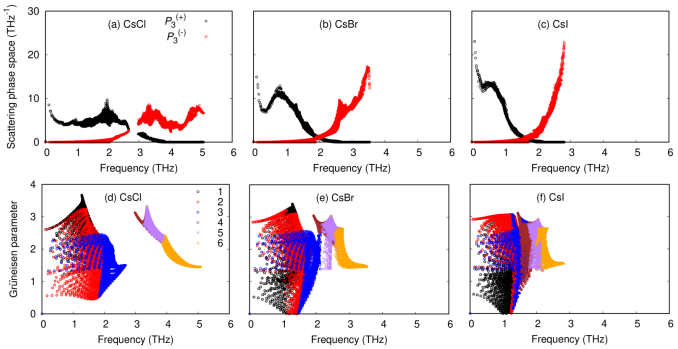

Fig. 2 Three-phonon scattering phase spaces for the absorption ($P_3^{(+)}$) and emission ($P_3^{(-)}$) processes in (a) CsCl, (b) CsBr and (c) CsI. The Grüneisen parameters of (d) CsCl, (e) CsBr and (f) CsI.

3 RESULTS AND DISCUSSION

The lattice constants of CsCl, CsBr and CsI computed in this work are 3.97, 4.15 and 4.41 Å, respectively, which are in reasonable agreement with the experimental values of 4.09 [26], 4.26 [27] and 4.56 Å [28]. The temperature-dependent k_L of CsX are given in Fig. 1a. The k_L of CsI is higher than those of CsCl and CsBr, which is contrary to the expectation that materials with heavier atoms usually exhibit lower k_L. Our calculated room temperature k_L of CsCl, CsBr and CsI are 1.38, 1.40 and 1.80 W/mK, respectively, which are higher than the experimental values [7]. The higher theoretical k_L may be related to the underestimation of the lattice constants, which will be discussed later with the pressure dependence of k_L.

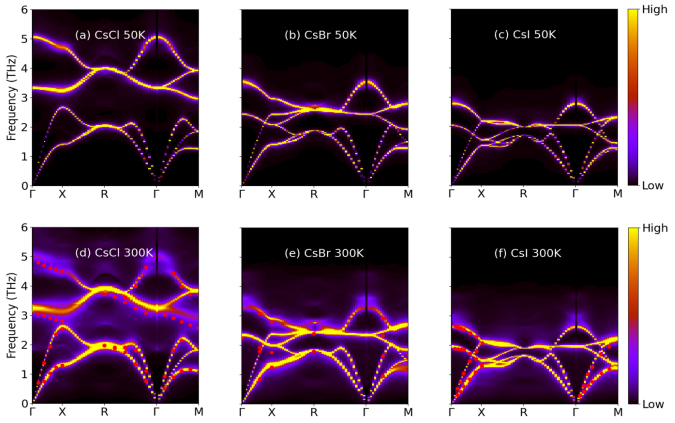

Fig. 3 Phonon spectra of CsCl, CsBr and CsI at 50 and 300 K. The experimental phonon frequencies at room temperature are given as red dots[10,26,31].

To better understand the anomalous thermal transport behavior of CsX, the cumulative k_L at 300 K are calculated, as shown in Fig. 1b. It is seen that, in the range of $1 \sim 2.1$ THz, the cumulative k_L of CsI is much larger. From the mode dependent k_L given in the inset of Fig. 1b, it is seen that the two TO modes have significant contributions to the thermal transport of CsI. For CsCl and CsBr, the thermal transport is dominated by the acoustic modes, which account for 90% and 85% of the k_L, respectively. While for CsI, the contribution from optical modes becomes much larger, and the acoustic modes only account for 67% of its k_L. Therefore, the larger k_L of CsI is closely related to the TO modes in the range of $1 \sim 2.1$ THz.

To further elucidate the microscopic mechanism of the thermal transport of CsX, the group velocities and phonon lifetimes at 300 K are calculated, as shown in Fig. 1c and 1d. The group velocities of all phonon modes are below 4000 m/s, which is comparable to the well-known low-k_L materials PbTe[29], SnSe[5] and BiCuSeO[30]. It is seen that the phonon group velocities of CsI are obviously lower than those of CsCl and CsBr, due to the softening of the phonon modes of CsI, as shown in Fig. s2a. A lower phonon group velocity contributes to a lower k_L; however, the phonon lifetimes of CsI are longer than those of CsCl and CsBr, especially for the modes in the range of $1 \sim 2.1$ THz, indicating that the anharmonic phonon-phonon interactions at this range are weaker in CsI. Therefore, the higher k_L of CsI can be ascribed to its longer phonon lifetimes.

We have further calculated the three-phonon scattering phase space P_3, which is defined as[15]:

$$P_3(q,j) = \frac{1}{3m^3}(2P_3^{(+)}(q,j) + P_3^{(-)}(q,j)) \tag{5}$$

where m is the number of phonon modes and

$$P_3^{\pm}(q,j) = \frac{1}{N_q}\sum_{q_1,q_2,j_1,j_2}\delta(\omega_{q,j} \pm \omega_{q_1,j_1} - \omega_{q_2,j_2})\delta_{q\pm q_1,q_2+G} \tag{6}$$

$P_3^{\pm}(q,j)$ describes two types of scattering events that satisfy the energy and momentum conservations, i.e., the absorption (+) and emission (-) processes. N_q is the number of q points involved, and G is the reciprocal lattice vector. The total scattering phase space can be calculated using the following equation[15]:

$$P_3 = \frac{1}{N_q}\sum_{q,j} P_3(q,j) \tag{7}$$

The total scattering phase spaces of CsCl, CsBr and CsI are calculated, and they are equal to 0.074, 0.069 and 0.053 THz^{-1}, respectively (see Fig. s3). The smaller phase space of CsI is consistent with its longer phonon lifetimes. Detailed scattering phase spaces for the absorption and emission processes are given in Fig. 2a-2c. It is seen that, the absorption processes are dominated by phonon modes at lower frequency range, while emission processes are contributed by phonon modes at higher frequency range. At frequency range of $0 \sim 1$ THz, the absorption processes of CsI are stronger than those of CsCl and CsBr, corresponding to the lower cumulative k_L at this range, as shown in Fig. 1b. While the absorption processes of CsI are weaker in the range of $1 \sim 2.1$ THz, which is consistent with its higher cumulative k_L in this range. The weaker absorption in this range may be attributed to the tight phonon bunching of CsI at 0 GPa. As shown in Fig. s2a, the bunched frequency region of CsI is located in the range of $1.2 \sim 2.2$ THz and the maximum phonon frequency is 2.8 THz, suggesting some three-phonon absorption processes are difficult to occur in the range of $1 \sim 2.1$ THz since energy conservation cannot be easily satisfied. Moreover, the Grüneisen parameters of CsX, which describe the volume dependence of phonon frequency and are related to the lattice anharmonicity, are calculated using the third-order force constants. It is known that materials with larger Grüneisen parameters usually possess stronger anharmonicity and exhibit lower k_L. As shown in Fig. 2d-2f, the Grüneisen parameters of CsI are smaller than those of CsCl and CsBr, suggesting weaker lattice anharmonicity and contributing to its higher k_L.

The finite-temperature phonon spectra of CsX are calculated and presented in Fig. 3. Phonon frequencies obtained from inelastic neutron scattering experiments are also given for comparison[10,26,31]. It is seen that our calculations are consistent with the experimental measurements. At 50 K, phonon spectra are sharp because of the weak phonon-phonon interactions. As temperature increases, broadening of phonon spectra is observed due to the enhanced phonon-phonon interactions. It is also found that in the range of $1 \sim 2.1$ THz, due to the weaker phonon-phonon scatterings in CsI, the phonon linewidths of CsI are smaller than those of CsCl and CsBr.

By further investigating the pressure effect, we find that the k_L of CsI is more sensitive to hydrostatic pressures. The room-temperature k_L of CsX has been calculated under -2, -1, 0, and 1 GPa. The comparison between our theoretical results and the experimental measurements[7] is given in Fig. 4a. The pressure-dependent k_L calculated in this work is in agreement with the experimental data once the theoretical pressure (P_{theo}) is offset by 1 GPa from the experimental pressure (P_{exp}) (i.e., P_{theo}=P_{exp}-1). Because of the well-known overbinding of LDA, the calculated lattice constants of CsCl, CsBr and CsI at -1 GPa (expansion) are

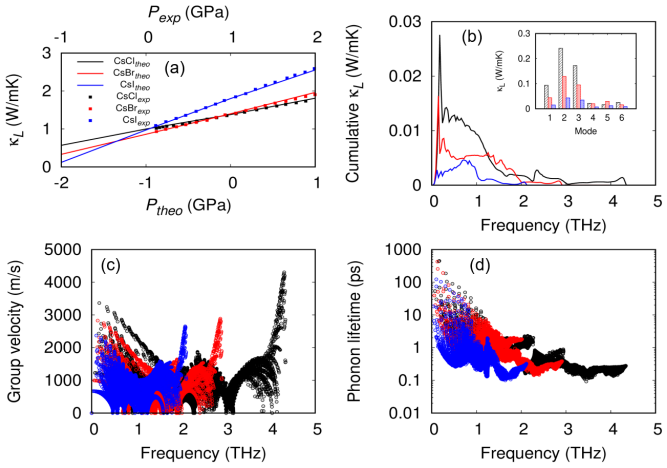

Fig. 4 Pressure-dependent room-temperature lattice thermal conductivities of CsCl, CsBr and CsI. Discrete dots represent experimental data extracted from Ref. [7]. Theoretical pressure (P_{theo}) is offset by 1 GPa from the experimental pressure (P_{exp}), i.e., P_{theo}=P_{exp}-1. (b) Room-temperature cumulative lattice thermal conductivity and mode-dependent lattice thermal conductivity (inset) of CsX at -2 GPa. Phonon group velocities (c) and room-temperature phonon lifetimes (d) of CsCl, CsBr and CsI at -2 GPa.

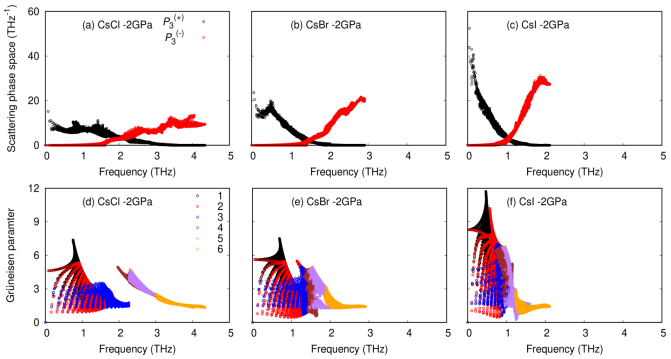

Fig. 5 Three-phonon scattering phase spaces for the absorption ($P_3^{(+)}$) and emission ($P_3^{(+)}$) processes in (a) CsCl, (b) CsBr and (c) CsI at -2 GPa. The Grüneisen parameters of (d) CsCl, (e) CsBr and (f) CsI at -2 GPa.

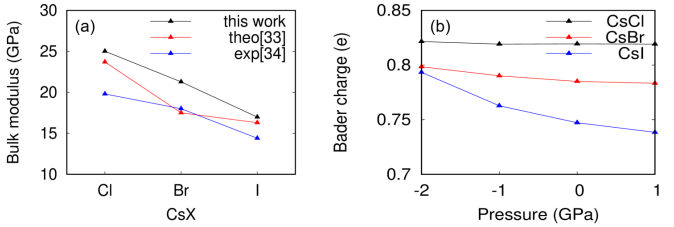

Fig. 6 (a) Bulk moduli of CsCl, CsBr, and CsI. Existing theoretical[32] and experimental data[33] are also shown for comparison. (b) Charge received by Cl, Br and I atoms obtained based on Bader charge analysis.

4.03, 4.22 and 4.51 Å, respectively, which are very close to the experimental values of 4.09[26], 4.26[27] and 4.56 Å[28] measured at ambient conditions. It is seen that the k_L of CsX increases under a compressive pressure of 1 GPa, and the increase in CsI is larger than that in CsCl and CsBr. When negative pressures (expansion) are applied, the k_L of CsI decreases more rapidly compared with those of CsCl and CsBr. At -2 GPa, we see that the order of k_L becomes CsCl $>$ CsBr $>$ CsI. The cumulative k_L of CsX at -2 GPa are given in Fig. 4b. In the entire frequency range, the cumulative k_L of CsI becomes lower than those of CsCl and CsBr. The lower k_L of CsI at -2 GPa is mainly due to the suppressed contributions from the acoustic phonon modes. The group velocities and room-temperature phonon lifetimes at -2 GPa are given in Fig. 4c and 4d, respectively. The group velocities of CsI are smaller than those of CsCl and CsBr at -2 GPa (see Fig. s2b). Contrary to that at 0 GPa, the room-temperature phonon lifetimes of CsI at -2 GPa are shorter than those of CsCl and CsBr, indicating stronger anharmonic phonon-phonon scatterings in CsI. Therefore, both the shorter phonon lifetimes and the smaller group velocities are responsible for the lower k_L of CsI at -2 GPa.

The three-phonon scattering phase spaces of CsX at -2 GPa are given in Fig. 5 to better understand their anharmonic phonon-phonon interactions. The total scattering phase spaces of CsCl, CsBr and CsI at -2 GPa are 0.10, 0.097 and 0.14 THz^{-1}, respectively (see Fig. s3). CsI has the largest total scattering phase space and the lowest k_L at -2 GPa. The scattering phase spaces for absorption processes in the range of 0 $\sim$ 1 THz in CsI are obviously larger than those of CsCl and CsBr, and the scattering phase spaces for emission processes in the range of 1 $\sim$ 2 THz are also larger in CsI. Compared with that at 0 GPa, the phonon bunching of CsI at -2 GPa becomes tighter, and the bunching moves down to the middle frequency region (Fig. s2b), indicating the energy conservation can be more easily satisfied, leading to stronger phonon-phonon scattering at -2 GPa. Therefore, the stronger anharmonic absorption and emission processes in CsI at -2 GPa play an important role on its lower k_L. The Grüneisen parameters of CsX at -2 GPa are also calculated. As shown in Fig. 5d-5f, the Grüneisen parameters of CsI are significantly larger than those of CsCl and CsBr, implying stronger lattice anharmonicity of CsI at -2 GPa, which contributes to its lower k_L.

Finally, the different pressure dependences of the k_L of CsX are discussed by analyzing the bulk modulus and Bader charge. As shown in Fig. 6a, the bulk moduli of CsCl, CsBr and CsI calculated in this work are 25.0, 21.3 and 17.0 GPa, respectively, which agree qualitatively with previous theoretical (23.7, 17.5, and 16.3 GPa[32]) and experiment results (19.8, 18.0, and 14.4 GPa[33]), indicating that CsI is more compressible than CsBr and CsI. The lattice constant of CsI also increases more rapidly under tensile stress, which contributes to its lower k_L at -2 GPa. In addition, due to the larger variation of Cs-I bond length under pressures, the electron transfer in CsI also changes more rapidly. It is seen from Fig. 6b that the Bader charge of I reduces more rapidly from -2 to 1 GPa, which may also affect the thermal transport property. It was reported that the ionicity related LO-TO splitting of a compound can affect the available three-phonon scattering channels and thus the lattice thermal transport[34].

4 CONCLUSIONS

In summary, the k_L of CsX (X = Cl, Br, I) and its pressure dependence are investigated from first-principles calculations. De-

spite the larger atomic mass of I, CsI exhibits higher k_L than CsCl and CsBr at ambient conditions. By analyzing the group velocity, phonon lifetime, three-phonon scattering phase space, and Grüneisen parameter, we attribute the higher k_L of CsI to its longer phonon lifetimes originated from weaker absorption processes in the range of $1 \sim 2.1$ THz. Finite temperature phonon spectra are calculated by considering the third-order anharmonicity. Furthermore, the pressure dependence of k_L is studied in the range of $-2 \sim 1$ GPa. We find that the k_L of CsI becomes the lowest at -2 GPa due to its shorter phonon lifetimes and smaller group velocities. Contrary to that at 0 GPa, the lattice anharmonicity of CsI at -2 GPa is stronger than those of CsCl and CsBr. Finally, the stronger pressure dependence of k_L of CsI is found to be related to its compressibility and electron transfer.

5 ACKNOWLEDGMENTS

This work is supported by the National Natural Science Foundation of China (Grant No. 12104234), Natural Science Foundation of Jiangsu Province (Grant Nos.BK20210578 and 20KJB140004 and JSSCBS20210513) and NUPTSF (Grant Nos. NY220096 and NY220204). YP acknowledges the National Natural Science Foundation of China (Grant No. 61874060, U1932159, 61911530220), Jiangsu Specially-Appointed Professor program, Natural Science Foundation of Jiangsu Province (Grant No. BK20181388, 19KJA180007) and Oversea Researcher Innovation Program of Nanjing, NUPTSF (Grant No. NY217118). The authors are grateful for the research computing facilities offered by ITS, HKU.

Notes and references

1 D. Morelli, V. Jovovic and J. Heremans, *Phys. Rev. Lett.*, 2008, **101**, 035901.

2 B. Li, H. Wang, Y. Kawakita, Q. Zhang, M. Feygenson, H. Yu, D. Wu, K. Ohara, T. Kikuchi, K. Shibata *et al.*, *Nat. Mater.*, 2018, **17**, 226–230.

3 P. Ying, X. Li, Y. Wang, J. Yang, C. Fu, W. Zhang, X. Zhao and T. Zhu, *Adv. Funct. Mater.*, 2017, **27**, 1604145.

4 O. Delaire, J. Ma, K. Marty, A. F. May, M. A. McGuire, M.-H. Du, D. J. Singh, A. Podlesnyak, G. Ehlers, M. Lumsden *et al.*, *Nat. Mater.*, 2011, **10**, 614–619.

5 C. W. Li, J. Hong, A. F. May, D. Bansal, S. Chi, T. Hong, G. Ehlers and O. Delaire, *Nat. Phys.*, 2015, **11**, 1063–1069.

6 S. Li, J. Ma, Y. Pei and Y. Chen, *J. Mater. Chem. C*, 2019, **7**, 5970–5974.

7 D. Gerlich and P. Andersson, *J. Phys. C: Solid State Phys.*, 1982, **15**, 5211.

8 R. W. Keyes, *Phys. Rev.*, 1959, **115**, 564.

9 M. Sist, K. F. F. Fischer, H. Kasai and B. B. Iversen, *Angew. Chem.*, 2017, **129**, 3679–3683.

10 B. Wei, X. Yu, C. Yang, X. Rao, X. Wang, S. Chi, X. Sun and J. Hong, *Phys. Rev. B*, 2019, **99**, 184301.

11 C. He, C.-E. Hu, T. Zhang, Y.-Y. Qi and X.-R. Chen, *Solid State Commun.*, 2017, **254**, 31–36.

12 L. Elalfy, D. Music and M. Hu, *Phys. Rev. B*, 2021, **103**, 075203.

13 S. Kawano, T. Tadano and S. Iikubo, *J. Phys. Chem. C*, 2021, **125**, 91–97.

14 Z. Yang, K. Yuan, J. Meng, X. Zhang, D. Tang and M. Hu, *Nanotechnology*, 2020, **32**, 025709.

15 T. Tadano and S. Tsuneyuki, *J. Phys. Soc. Japan*, 2018, **87**, 041015.

16 S. Li and Y. Chen, *Phys. Rev. B*, 2017, **96**, 134104.

17 F. Zhou, W. Nielson, Y. Xia, V. Ozoliņš *et al.*, *Phys. Rev. Lett.*, 2014, **113**, 185501.

18 T. Tadano, Y. Gohda and S. Tsuneyuki, *J. Phys. Condens. Matter*, 2014, **26**, 225402.

19 T. Tadano and S. Tsuneyuki, *Phys. Rev. B*, 2015, **92**, 054301.

20 L. J. Nelson, G. L. Hart, F. Zhou, V. Ozoliņš *et al.*, *Phys. Rev. B*, 2013, **87**, 035125.

21 T. Goldstein and S. Osher, *SIAM j. Imaging Sci.*, 2009, **2**, 323–343.

22 G. Kresse and J. Furthmüller, *Comput. Mater. Sci.*, 1996, **6**, 15–50.

23 P. E. Blöchl, *Phys. Rev. B*, 1994, **50**, 17953.

24 W. Kohn and L. J. Sham, *Phys. Rev.*, 1965, **140**, A1133.

25 H. J. Monkhorst and J. D. Pack, *Phys. Rev. B*, 1976, **13**, 5188.

26 A. Ahmad, H. Smith, N. Wakabayashi and M. Wilkinson, *Phys. Rev. B*, 1972, **6**, 3956.

27 V. Ganesan and K. Girirajan, *Pramana*, 1986, **27**, 475–478.

28 W. Bühner and W. Hälg, *phys. Status Solidi B*, 1971, **46**, 679–686.

29 Z. Tian, J. Garg, K. Esfarjani, T. Shiga, J. Shiomi and G. Chen, *Phys. Rev. B*, 2012, **85**, 184303.

30 Y.-L. Pei, J. He, J.-F. Li, F. Li, Q. Liu, W. Pan, C. Barreteau, D. Berardan, N. Dragoe and L.-D. Zhao, *NPG Asia Mater.*, 2013, **5**, e47–e47.

31 S. Rolandson and G. Raunio, *Phys. Rev. B*, 1971, **4**, 4617.

32 A. Y. Kuznetsov, A. Sobolev, A. Makarov and A. Velichko, *Phys. Solid State*, 2005, **47**, 2030–2034.

33 W. Mei, L. Boyer, M. Mehl, M. Ossowski and H. Stokes, *Phys. Rev. B*, 2000, **61**, 11425.

34 S. Mukhopadhyay and D. A. Stewart, *Phys. Rev. Lett.*, 2014, **113**, 025901.